ELSEVIER

International Journal of Heat and Fluid Flow 22 (2001) 123–133

International Journal of HEAT AND FLUID FLOW

www.elsevier.com/locate/ijhff

The effect of turbulence intensity and length scale on low-pressure turbine blade aerodynamics

Robert J. Butler [a,*], Aaron R. Byerley [b], Kenneth VanTreuren [c], James W. Baughn [d]

[a] *Propulsion Development System Office, Aeronautical Systems Center, Wright-Patterson AFB, Bldg. 28, Room 201, 2145 Mohahan Way, OH 45433-7017, USA*

[b] *Department of Aeronautics, USAF Academy, Colorado Springs, CO, USA*

[c] *Department of Engineering, Baylor University, Waco, TX, USA*

[d] *Mechanical and Aeronautical Engineering, University of California, Davis, CA, USA*

Received 15 March 2000; accepted 3 October 2000

Abstract

Unpredicted losses have been observed in low-pressure gas turbine stages during high altitude operation. These losses have been attributed to aerodynamic separation on the turbine blade suction surfaces. To gain insight into boundary layer transition and separation for these low Reynolds number conditions, the heat transfer distribution on a Langston turbine blade shape was measured in a linear cascade wind tunnel for turbulence levels of 0.8% and 10% and Reynolds numbers of 40–80*k*. Turbulence levels of 10% were generated using three passive biplanar lattice grids with square-bar widths of 1.27, 2.54 and 6.03 cm to investigate the effect of turbulence length scale. The heat transfer was measured using a uniform heat flux (UHF) liquid crystal technique. As turbulence levels increased, stagnation heat transfer increased and the location of the suction-side boundary layer transition moved upstream toward the blade leading edge. For this turbine blade shape the transition location did not depend on turbulence length scale, the location is more dependent on pressure distribution, Reynolds number and turbulence intensity. For the 10% turbulence cases, the smaller length scales had a larger affect on heat transfer at the stagnation point. A laser tuft method was used to differentiate between boundary layer transition and separation on the suction surface of the blade. Separation was observed for all of the low turbulence (clean tunnel) cases while transition was observed for all of the 10% turbulence cases. Separation and transition locations corresponded to local minimums in heat transfer. Reattachment points did not correspond to local maximums in heat transfer, but instead, the heat transfer coefficient continued to rise downstream of the reattachment point. For the clean tunnel cases, streamwise streaks of varying heat transfer were recorded on the concave pressure side of the turbine blade. These streaks are characteristic of either Görtler vortices or a three-dimensional transition process. For the 10% turbulence cases, these streaks were not present. The results presented in this paper show that turbulence length scale, in addition to intensity have an important contribution to turbine blade aerodynamics and are important to CFD modelers who seek to predict boundary layer behavior in support of turbine blade design optimization efforts.

1. Background

This work provides insight into the detailed aerodynamics associated with a low-pressure turbine operating at low Reynolds number. Due to gas turbine engines operating over a large range of atmospheric pressures and airspeeds from takeoff to cruise altitude, unexpected aerodynamic losses occur during low Reynolds number operation. Flow separation reduces the operating efficiency of the low-pressure turbine which results in increased fuel consumption. As noted by Rivir (1996), "unpredicted losses in the low-pressure turbine during operation at high altitudes has stimulated current interest in transition and separation at low Reynolds numbers".

Although actual turbine rotor blade aerodynamics are three-dimensional and take place in an extreme environment (high temperature and turbulence), little fundamental research on turbine blades is performed in operating gas turbine engines due to practical limitations. Instead, different types of experimental approaches are used to simplify studies of the flow and heat transfer in turbine stages. In general, these different approaches are divided into two categories, cascade (linear and annular) and rotating facilities. The cascade and rotating facilities can be further subdivided depending on whether they use steady-state or transient testing techniques. For a review of these techniques, see Baughn et al. (1995).

The present experiments were conducted in a steady-state linear cascade. Steady-state linear cascade research started with very early work by Wilson and Pope (1954). The United Technologies Research Center (UTRC) group ran important test cases using a now common blade shape in a linear cascade

* Corresponding author. Tel.: +1-937-255-2300 ext. 3029.
E-mail address: robert.butler@wpafb.af.mil (R.J. Butler).

0142-727X/01/$ - see front matter
PII: S0142-727X(00)00081-3

Notation

b_x	airfoil axial chord (m)
B_1	air inlet angle (°)
B_2	air exit angle (°)
h	local heat transfer coefficient (W/m^{2}K)
i	electric current (A)
l	length of gold sheet (m)
Nu	Nusselt number based on axial chord
P_{atm}	atmospheric pressure (kPa)
p	pitch distance between turbine blades (m)
q''	total heat flux (W/m^2)
q''_c	convective heat flux (W/m^2)
q''_L	conductive heat loss (W/m^2)
$R(t)$	autocorrelation function
Re	Reynolds number based on inlet conditions and axial chord
R_{35}	resistance of gold at 35.6°C (Ω)
R''_{35}	resistance per square of gold at 35.6°C (Ω/sq.)
s	surface arc length (m)
t	time (s)
T_∞	free-stream air temperature (°C)
T_{LC}	temperature when liquid crystal is yellow (35.6°C)
Tu	turbulence intensity
$\overline{U}$	mean velocity in the x-direction (m/s)
w	width of gold film (m)
x	distance measured in the axial chord direction (m)
y	distance measured perpendicular to axial chord (m)

Greeks

β	cascade flow angle measured relative to the y-axis (°)
ϵ	surface emissivity
σ	Stefan–Boltzman constant (W/m^{2}K^4)
Λ_x	macro length scale in x-direction (m)
λ	micro length scale in x-direction (m)

(Langston et al., 1977; Graziani et al., 1980), later they used this same shape in rotating tests. This blade shape is commonly referred to as the Langston blade and was used in the present experiments. Detailed aerodynamic measurements were performed on the Langston geometry at Virginia Polytechnic Institute (Moore and Ransmayr, 1984a,b; Moore and Adhye, 1985; Moore and Moore, 1985; Moore et al., 1987). Heat transfer data were collected on the Langston geometry at NASA Lewis (Hippensteele et al., 1985; Boyle and Russell, 1990) and numerical computations were performed by Boyle (1991). Turbulence and wake effects were also studied in the linear cascade test facility at the Institute of Thermal Turbomachinery (ITS), Karlsruhe, Germany by Dullenkopf et al. (1991) and Dullenkopf and Mayle (1994). Zhang and Han (1994) measured the effect of turbulence on turbine blade heat transfer using Reynolds numbers ranging from 100,000 to 300,000.

The current research used a uniform heat flux (UHF) or heated-coating method to measure the heat transfer. This method determines local heat transfer coefficients by measuring the local surface temperatures on a model with a uniform heat transfer flux produced from a heated-coating on the test surface. The local heat transfer coefficient is calculated from the known power into the surface, local surface temperature, and free-stream temperature. Variations on the UHF technique involve different ways to measure the surface temperature and different ways to produce the heat flux. Many researchers have used UHF methods. Early work using this technique used thermocouples to measure the local surface temperature. For example, local heat transfer coefficients were measured on a cylinder in cross-flow by Giedt (1949) using thermocouples to measure surface temperature and nichrome ribbon to produce the electrical resistance heat flux. Wilson and Pope (1954) used a similar technique while measuring the heat transfer on turbine blade shapes in very early cascade tunnel testing. Simonich and Bradshaw (1978) used steel shim strips to produce the needed heat flux to measure the effect of free-stream turbulence on turbulent boundary layers. O'Brien et al. (1986) used inconel foil and thermocouples on one of their three different cylinder models used to compare different heat transfer techniques. More recent techniques have used liquid crystals on the test surface to measure the surface temperature. Cooper et al. (1975) used carbon impregnated paper to produce the heat flux and liquid crystals to test a cylinder in cross-flow. A similar technique was used by Hippensteele et al. (1985) to measure the local heat transfer around a turbine blade in a cascade tunnel. As with the present method, Baughn et al. (1989) used a thin polyester surface with vacuum-deposited gold and liquid crystals to compare UHF and transient tests on a pin fin. Endwall heat transfer in a cascade tunnel was investigated by Boyle and Russell (1990) using a thin metallic foil and liquid crystals. Graziani et al. (1980), Dring et al. (1986), Blair et al. (1989a), Blair et al. (1989b) and Blair (1994) used this technique with thermocouples to measure surface temperature. Like the present method, Hippensteele et al. (1985) and Boyle and Russell (1990) used liquid crystals to measure surface temperature. The present research uses gold-film for the heater and liquid crystals to measure temperature similar to that of Baughn et al. (1989) and Baughn et al. (1995).

The purpose of the present work was to determine the effect of turbulence intensity, length scale, and Reynolds number on the heat transfer distribution of a turbine blade at a low Reynolds number (40,000–80,000 based on inlet conditions). The heat transfer distribution provides insight into boundary layer transition and separation on the blade. The heat transfer distributions are complimented with Laser Thermal Tuft measurements which show local surface flow direction to determine the difference between regions of flow separation from transition. Murawski et al. (1997) used hot-wire anemometry measurements to look at the separation region on a turbine blade under similar conditions to the present work. With their geometry, they experienced boundary layer separation for all of their cases regardless of Reynolds number or turbulence intensity. They found that increasing the Reynolds number, without changing freestream turbulence, resulted in a slight rearward movement of the separation point and shrinkage of the separation zone. Huang and Xiong (1998) incorporated intermittency, along with Reynolds number and turbulence intensity to compute detailed flow separation conditions on a turbine blade under low Reynolds number conditions. Van Fossen et al. (1995) investigated the effects of turbulence intensity, length scale, Reynolds number and leading edge velocity gradient on stagnation heat transfer. Van Fossen et al. (1995) showed length scale to be more important than velocity gradient and they developed a correlation using intensity, length scale, and Reynolds number. Their work showed heat transfer increasing with smaller length scale. Mayle et al. (1997) predicts that an optimal frequency exists for enhancing heat transfer, which is produced by an optimal length scale. The current study expands on previous work by emphasizing the turbulence length scale and its effect on the turbine blade heat transfer and aerodynamics.

2. Experimental apparatus

The test facility at the US Air Force Academy (USAFA) is a closed loop wind tunnel facility specifically designed for use as a linear cascade. The tunnel is capable of velocities from 5 m/s up to approximately 75 m/s, and is adjusted by moving variable pitch fan blades on a 200 Hp electric motor. The tunnel operates near ambient pressure and temperature (typically 78 kPa and 22–25°C). The temperature can be controlled. For the requirements of this study the lowest tunnel speeds were used. The geometry of the linear cascade sections and of the turbine blades are shown in Figs. 1 and 2. The parameters for Fig. 1 are shown in Table 1. The x-axis is defined in the axial direction and cascade angles are defined relative to the y-axis. The USAFA tunnel was modified to accept seven blades (nine including sidewalls) with a high aspect ratio of 3.97 which achieves uniform two-dimensional flow over the test portion of the blades. The Langston turbine blade geometry, shown in Fig. 2, is very well documented in the literature. The blade shape is that of a heavily loaded machine with a design flow coefficient of 0.78, stage loading coefficient of 2.8, and 34% static pressure reaction (Blair et al., 1989a,b). The turbine blade has an inlet mean camber line angle of 44° and an exit mean camber line of 26°. The air inlet angle is 46°.

Locations on the turbine blade were measured relative to a geometric zero, which is determined by placing a straight edge across the concave portion of the turbine blade. The tangent point near the leading edge is used as the reference point ($s = 0$). Note, this location is not the stagnation point, although, this reference location is easier to duplicate and is consistent with Blair et al. (1989a,b). The clean tunnel freestream turbulence was measured with a hot-wire to be 0.4–0.8% depending on Reynolds number.

The center heat transfer blade was cut from dense (32 kg/m^3) polystyrene foam ($k = 0.027$ W/m K) using a hot-wire. Heat transfer tests were performed on the center blade in the cascade row. The blades on either side of the heat transfer test blade were tapped to measure static pressure over each blade.

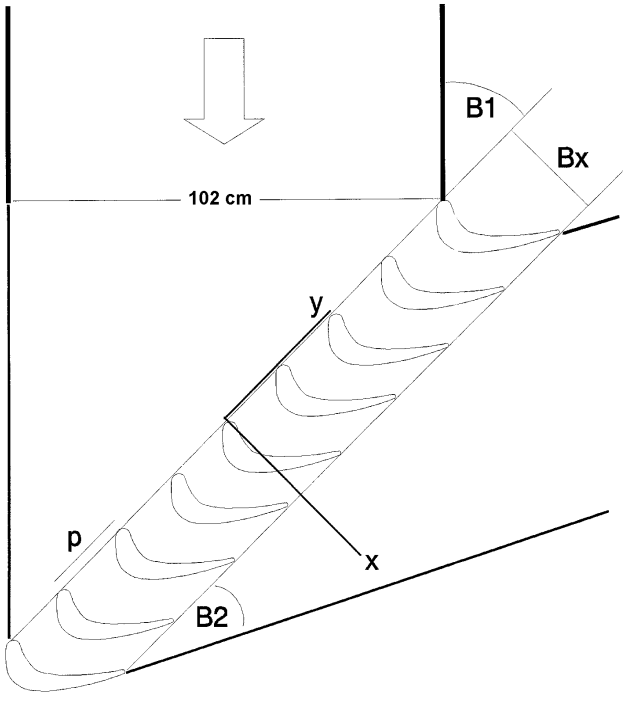

Fig. 1. Cascade geometry.

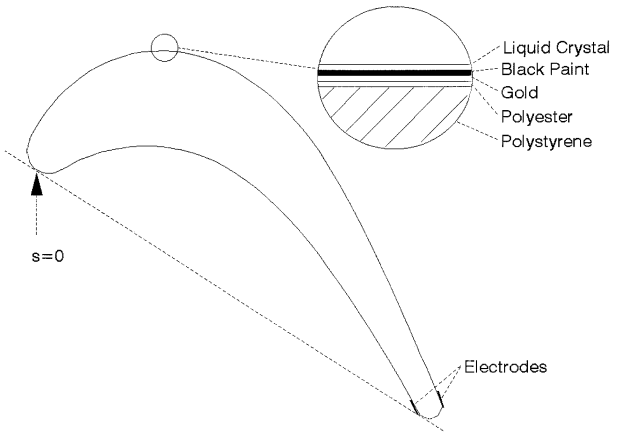

Fig. 2. Langston turbine blade geometry.

Table 1
Cascade parameters

Operation	Closed loop
Axial chord (b_x)	0.171 m
Blade pitch (p)	0.163 m
Pitch/axial chord	0.95
Span/axial chord	3.86
Inlet camber angle	44°
Exit camber angle	26°
Air inlet angle (B_1)	46°
Air exit angle (B_2)	26°
Grid orientation	Perpendicular to freestream

For the heat transfer measurements, gold film was attached to the substrate (polystyrene) using a 3-M spray adhesive (see Fig. 2). The gold film is a 5-mil polyester sheet with vacuum-deposited gold on the surface. The thin layer of gold provides the surface with a uniform electrical resistivity. Bus bars (electrodes) were formed using copper tape attached to both sides of the trailing edge of the gold film. To ensure good electrical contact, a silver-based paint was applied between the copper tape and the gold film.

Elevated turbulence levels were generated using three passive biplanar lattice grids with square-bar widths of 1.27, 2.54 and 6.03 cm. In each case, the grids were placed the appropriate distance upstream of the test section to produce 10% turbulence intensity. Although the turbulence intensity was constant, the length scales of turbulence varied significantly due to the different grid-bar widths. The test conditions associated with each run are given in Table 2.

3. Experimental method

During the setup for each configuration, the tunnel periodicity was checked by measuring the pressure distribution of two blades, one on each side of the centered heat transfer blade. A typical pressure distribution is shown in Fig. 3.

Turbulence intensity and length scale data were collected using a constant temperature hot-film anemometer (IFA 300). To find the macro and micro length scales, an autocorrelation of the velocity data was performed. The hot-wire was located upstream of the blade row and the grid positioned accordingly to achieve the desired turbulence intensity at the hot-wire. After turbulence intensity and length scale data were collected,

Table 2
Test conditions

Grid size	*Re* (inlet conditions)	Turbulence (%)	Turb micro-scale, λ (mm)	Turb macro-scale, Λ (mm)
Clean tunnel	45,000	0.8		
Clean tunnel	77,300	0.4		
1.27-cm grid	44,400	10.1	16	40
1.27-cm grid	66,000	9.7	19	40
2.54-cm grid	46,100	10.1	20	58
2.54-cm grid	68,600	10.0	23	68
6.03-cm grid	42,300	10.0	25	81
6.03-cm grid	66,100	10.1	31	117

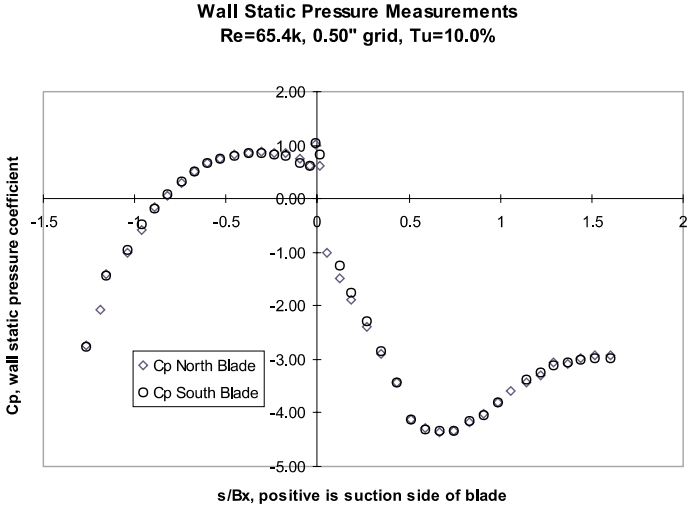

Fig. 3. Pressure distribution showing tunnel periodicity among blades.

the grid was moved closer to the blade row to produce the same turbulence intensity and length scale at the leading edge of the heat transfer blade.

A complete description of the steady-state liquid crystal technique can be found in Baughn et al. (1995). In this technique electric power was applied to the gold film covering on the heat transfer blade. A thin layer of black paint was applied over the gold film followed by R35W1 liquid crystals. The yellow isotherm of the crystal was calibrated to be 35.70°C (±0.15°C). During heat transfer testing, the chordwise location of the yellow isotherms were recorded, along with the corresponding electrical power supplied to the gold film. These data were then used to calculate the local heat transfer coefficients. By varying the electric power setting to the gold film, heat transfer coefficients were mapped over the entire blade.

4. Data reduction

Calculation of the macro and micro length scales for turbulent flow was done according to the method described in Roach (1987). The macro length scale for each flow was determined using the following equation:

$$\Lambda_x = \overline{U}\int_0^\infty R(t)\,\mathrm{d}t, \tag{1}$$

where $R(t)$ is the autocorrelation function. The autocorrelation function was numerically integrated from time zero until the first time the autocorrelation function was 0.

For the micro length scale, an autocorrelation of the velocity data was again accomplished. From Roach (1987), the micro length scale equation is

$$\lambda_x = \overline{U}\sqrt{\frac{-2}{\left(\partial^2 R(t)/\partial t^2\right)_{t=0}}}. \tag{2}$$

The first two temporal terms of the autocorrelation are used to approximate the second derivative. This can be done because the autocorrelation function is symmetric. Knowing that the autocorrelation function is 1.0 when time equals zero, the second derivative term is determined to be $(2R(\Delta t) - 2.0)/\Delta t^2$ from a finite-difference solution.

To determine the local heat transfer coefficients, a gold-film heated-coating (UHF) method was used. The voltage across the gold film was adjusted to increase or decrease local surface temperatures. The power level was adjusted to produce a liquid crystal isotherm at desired locations along the blade. At steady state, the liquid crystal isothermal lines map lines of constant heat transfer coefficient. The local heat transfer coefficient at the isotherm T_{LC} is then determined by

$$h = \frac{q''_c}{(T_{LC} - T_\infty)}. \tag{3}$$

A thermocouple exposed to the free-stream tunnel air was used to measure freestream temperature (T_∞). For the low Mach number flow of the present study, the measured temperature is within 0.1°C of the total, static, and adiabatic wall temperatures. The heat flux due to convection (q''_c) is determined by

subtracting radiation losses and conduction losses (q''_L) from the local heat flux (q''):

$$q''_c = q'' - \varepsilon\sigma(T^4_{LC} - T^4_\infty) - q''_L. \quad (4)$$

The local electrical heating varies slightly due to resistance variations of the gold coating with temperature. In the present method, this variation can be ignored since the data are all collected at the same isotherm temperature. Using the resistance of the gold coating at the yellow isotherm (35.70°C) and assuming the current is uniform through the model allows the local heat flux at the isotherm to be calculated

$$q'' = \frac{i^2 R_{35}}{lw} = \frac{i^2 (R''_{35} l/w)}{lw} = \frac{i^2 R''_{35}}{w^2}. \quad (5)$$

Note that the local heat flux depends only on the electric current, the gold sheet width, and the local resistance per square at the isotherm (in this case the resistance per square at the liquid crystal temperature of 35.7°C).

The electric current, length and width of the gold are measured. The resistance of the gold at 35.7°C (R_{35}) was expressed in terms of the resistance per square (R''_{35}). This resistance per square is a common way to express the resistance of surface coatings (note: due to scaling of the electrical path, any size square piece will have the same total resistance from side to side). The actual resistance of a rectangular piece is proportional to its length and inversely proportional to its width. The resistance of the gold sample was measured using a four-wire arrangement to be 5.707 Ω at 22°C. Baughn et al. (1985) measured the temperature coefficient of a similar gold coating to be 0.0011 (1/°C). Therefore, the resistance of the coating at 35.7°C would be $R_{35} = 5.707(1 + 0.0011(35 - 22)) = 5.79$ Ω. Accounting for the dimensions of the gold yields $R''_{35} = R_{35}(w/l) = 2.512$ Ω/sq. This method for data reduction accounts for the change of resistance with temperature (which is relatively small) but does not account for non-uniformities in the surface resistance due to variations in the thickness of the gold coating. This non-uniformity is included in the uncertainty analysis (see Table 2) and is assigned an uncertainty of 5%. Although no measurements were made of the uniformity for the particular batch of gold coatings used in the present study, previous experience with this material suggests that this is a conservative estimate. This is supported by the fact that the liquid crystals produced nearly straight lines along the length of the blades.

The conduction losses (q''_L) are small and are neglected for the polystyrene cascade blades used in this work. Radiation, however, cannot be ignored. The radiation component ranged from 3% in regions of very high convective heat transfer to 21% in regions of very low convective heat transfer.

5. Uncertainty analysis

An uncertainty analysis [using standard uncertainty methods of Kline and Mcklintock (1953), and 95% confidence] was performed for the heat transfer measurements. The individual contributions to the uncertainty of the plotted heat transfer data ($Nu/Re^{1/2}$) are given in Table 3 for the minimum and maximum power settings of 2.0 and 5.0 A. The non-uniformity of the gold's local resistivity, estimated to be approximately 5%, is the largest contributor to the overall uncertainty. The total uncertainty in the heat transfer is 5.86% at 5.0 A and 9.15% at 2.0 A. It is believed that this is conservative since the uniformity of the liquid crystal color during the tests suggest that the gold uniformity is probably much better than the 5% estimate. Physical measurements like stream-wise distance are accurate to 2 mm. The uncertainty in the coefficient of pressure is 5%.

6. Results

6.1. Effect of turbulence length scale on turbine blade heat transfer

Fig. 4 compares the stagnation point heat transfer coefficient for six different test conditions. In each case the turbulence intensity was roughly 10%, but the turbulence length scale was varied using three different grids and the tests were performed at two airspeeds to vary Reynolds number. Fig. 4 shows that the effect of increasing turbulence is magnified at higher Reynolds number. This conclusion is not new and has been shown by many researchers. At constant Reynolds number, the effect of length scale can also be determined. The

Table 3
Measurement uncertainty for 5.00 and 2.00 A current

				Units	% Uncertainty in $Nu/Re^{1/2}$
Current	5.00	±	0.005	A	0.21
Resistance	2.51	±	0.1256	Ω/sq.	5.20
Film width	0.20	±	0.0002	m	0.20
T_{inf}	25.0	±	0.15	°C	1.45
T_{LC}	35.75	±	0.15	°C	1.46
Emmisivity	0.85	±	0.15		0.70
Re	40,000	±	1320		1.60
Total					5.86%
Current	2.00	±	0.005	A	0.66
Resistance	2.51	±	0.1256	Ω/sq.	6.57
Film width	0.20	±	0.0002	m	0.26
T_{inf}	25.0	±	0.15	°C	1.82
T_{LC}	35.75	±	0.15	°C	1.87
Emmisivity	0.85	±	0.15		5.54
Re	40,000	±	1320		1.60
Total					9.15%

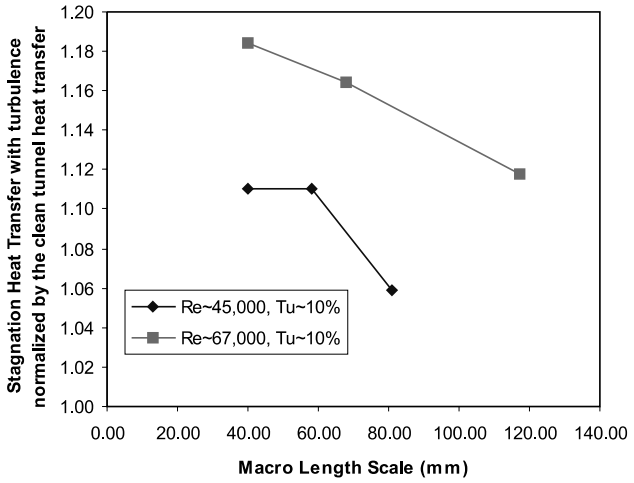

Fig. 4. The effect of Reynolds number and turbulence length scale on stagnation heat transfer at constant turbulence intensity (10%).

present data show that the turbulence length scale decreases as the stagnation heat transfer increases. Mayle et al. (1997) suggested "the idea of introducing an effective turbulence level was based on the fact that only the turbulence within a small band of frequencies can really affect the boundary layer since any turbulence at higher frequencies will be viscously damped, while that at lower frequencies will appear quasi-steady and have no time-averaged effect". The present results support Mayle's theory. In the present study the smallest length scales were closer to the optimal frequency for increasing heat transfer, but the length scale did not become small enough to confirm an optimal frequency. This is consistent with Van Fossen et al. (1995) who also found stagnation heat transfer to increase with decreasing length scale, without an optimal length scale being achieved.

Fig. 5 shows the heat transfer distribution ($Nu/Re^{0.5}$) over the entire turbine blade for four cases all near 45,000 Reynolds number. One case is for a clean tunnel and the other three cases have 10% turbulence at different length scales. The results at the stagnation point were discussed previously in Fig. 4. On the suction surface the boundary layer remains laminar until the minimum heat transfer location. In each case, 10% turbulence increases the heat transfer in this laminar region and the data overlay one another, without evidence of an effect due to length scale. The boundary layer then transitions from laminar to turbulent at $s/bx = 1.076$ for the smallest grid and $s/bx = 1.057$ for the other two grids. The clean tunnel case has a minimum heat transfer point at $s/bx = 1.168$, where the boundary layer separates, rather than transitions in the cases with grid generated turbulence. The laser tuft method was used to differentiate between boundary layer separation and transition. This method is explained later and is shown in Fig. 8.

On the pressure surface, all of the 10% turbulence cases look similar with a transition point. For the clean tunnel results on the pressure surface, the liquid crystal surface displayed stationary spanwise variation of local heat transfer levels described as "colored fingers" by Baughn et al. (1995) (see Fig. 6). Crane and Sabzvari (1989) observed similar "fingers" on a concave surface in a water tunnel. They attribute the fingers to Görtler vortices. The fingers begin where the strong concave curvature of the pressure side begins. The high heat transfer regions (fingers) are produced by downflow between vortices and the low heat transfer regions are formed by upflow (Baughn et al., 1995). The present study did not confirm if these fingers are Görtler vortices, but an alternate explanation for these variations could simply be a three-dimensional transition process. The high sensitivity of the liquid crystal technique allows for the detection of these fingers. Figs. 5 and 7 display the effects of these spanwise variations in heat transfer by showing the maximum and minimum heat transfer for any s/bx location on the pressure surface. For all of the grid generated turbulence cases the fingers disappear.

Fig. 7 shows the heat transfer distribution ($Nu/Re^{0.5}$) over the turbine blade for four cases near 68,000 Reynolds number. One case is for a clean tunnel and the other three cases have 10% turbulence at different length scales. The results at the stagnation point were discussed previously in Fig. 4. On the suction surface the boundary layer remains laminar until the minimum heat transfer location. In each case, 10% turbulence increases the heat transfer in this laminar region and

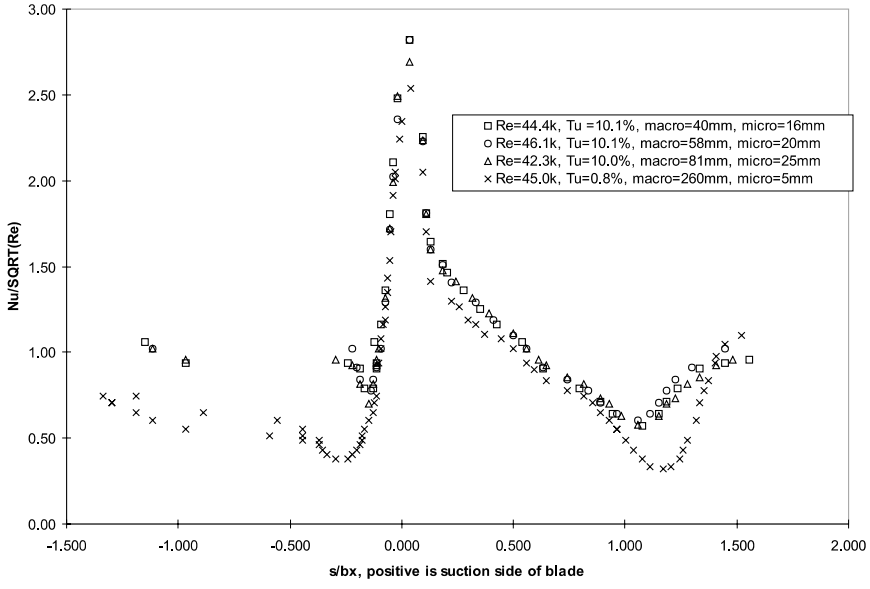

Fig. 5. The effect of turbulence length scale on turbine blade heat transfer ($Re \sim 45,000$).

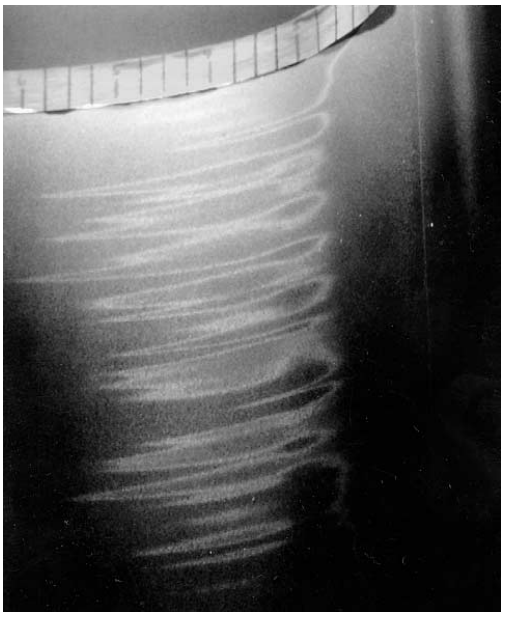

Fig. 6. Fingers of heat transfer variation on the pressure surface.

for this case of higher Reynolds number, it is evident that the largest length scale has the least amplification of the heat transfer. This is consistent with the stagnation heat transfer results discussed in Fig. 4. The boundary layer then transitions from laminar to turbulent at $s/bx = 1.002$ for all three grid turbulence cases. Once again, the turbulence length scale did not affect the transition location. The transition location is more dependant on Reynolds number and turbulence intensity. The clean tunnel case has a minimum heat transfer point at $s/bx = 1.113$, where the boundary layer separates, rather than transitions in the cases with grid generated turbulence. The pressure surface heat transfer profile is similar to the results discussed in Fig. 5 and the clean tunnel case exhibited Görtler vortices or three-dimensional transition.

In both Figs. 5 and 7, it is difficult to determine if the minimum heat transfer point on the suction surface is attributed to boundary layer transition or separation. It is extremely important to make this determination. In Fig. 8 the minimum heat transfer point is magnified in order to compare two cases of boundary layer separation to a case where the boundary layer transitioned.

Images of thermal laser tufts are shown in Fig. 8 to reveal flow direction. The laser tuft works by heating a very small spot on a liquid crystal surface with an IR laser. The IR laser saturates the red color in a RGB camera and shows up on the image as a round dot. Energy is advected away from the laser spot in the surface flow direction and this produces a "comet tail" in the surface flow direction due to the liquid crystal changing colors. In a reverse flow area, the "tail" will point upstream. At the separation point or a reattachment point, the laser tuft shows the laser circle surrounded by another circle signifying the lack of a preferred flow direction. Fig. 8 shows two cases at roughly 45,000 Reynolds number, one case is with a clean tunnel and the other case has 10% grid turbulence. For the clean tunnel case (0.8% turbulence) the boundary layer separates at $s/bx = 1.12$, reattaches at $s/bx = 1.37$, and has reverse flow in between. This is a very large separation zone and the heat transfer coefficient continues to rise downstream of the reattachment point. This observation associated with the reattachment point heat transfer is consistent with work reported by Rivir et al. (1994). Even at a fairly low Reynolds number (46,100), with 10% turbulence the boundary layer does not separate, but instead transitions from laminar to turbulent as shown by the top case in Fig. 8. For the clean tunnel case (0.4% turbulence) at higher Reynolds number (77,300) the boundary layer separates at $s/bx = 1.11$, reattaches at $s/bx = 1.21$, and has reverse flow in between. The increase in Reynolds number decreased the size of the separation zone by 56%.

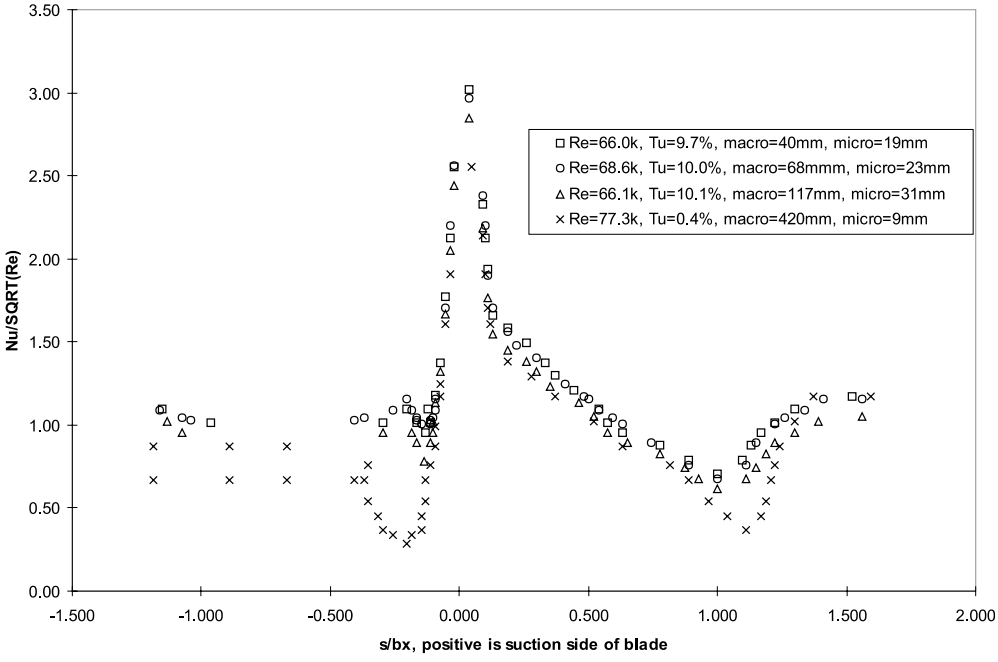

Fig. 7. The effect of turbulence length scale on turbine blade heat transfer ($Re \sim 68,000$).

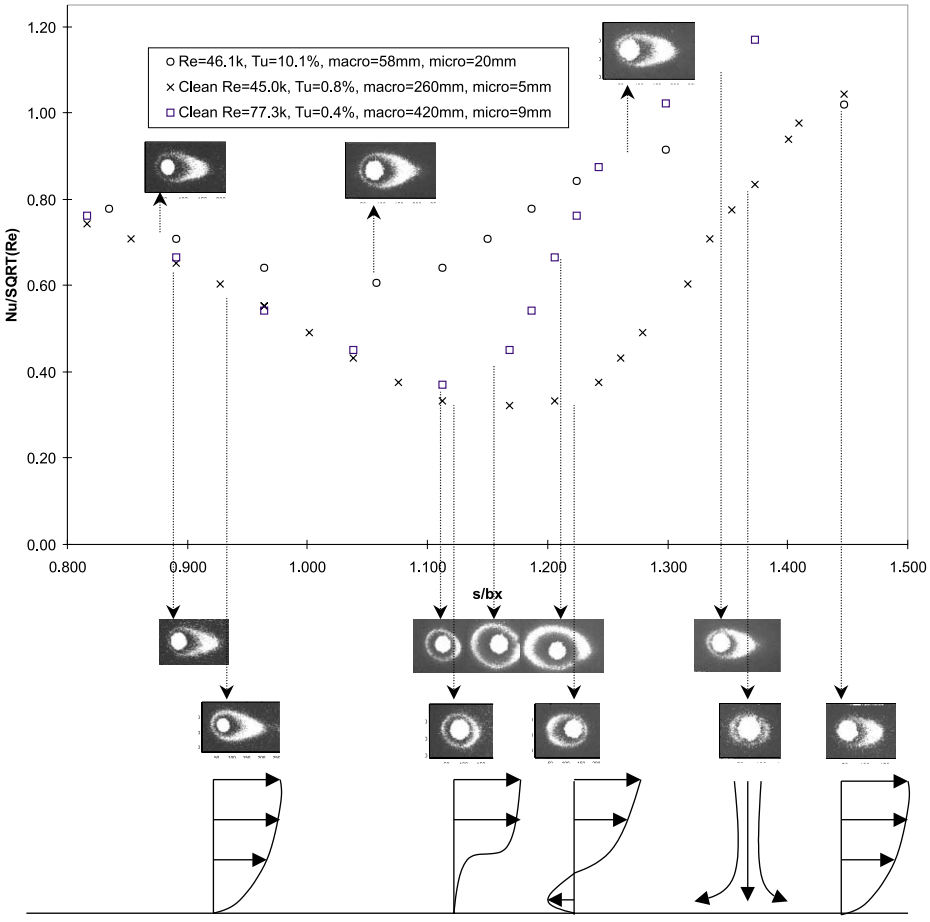

Fig. 8. Area of minimum heat transfer on the blade suction side with Laser Tuft images distinguishing between two cases of boundary layer separation from the top case of boundary layer transition.

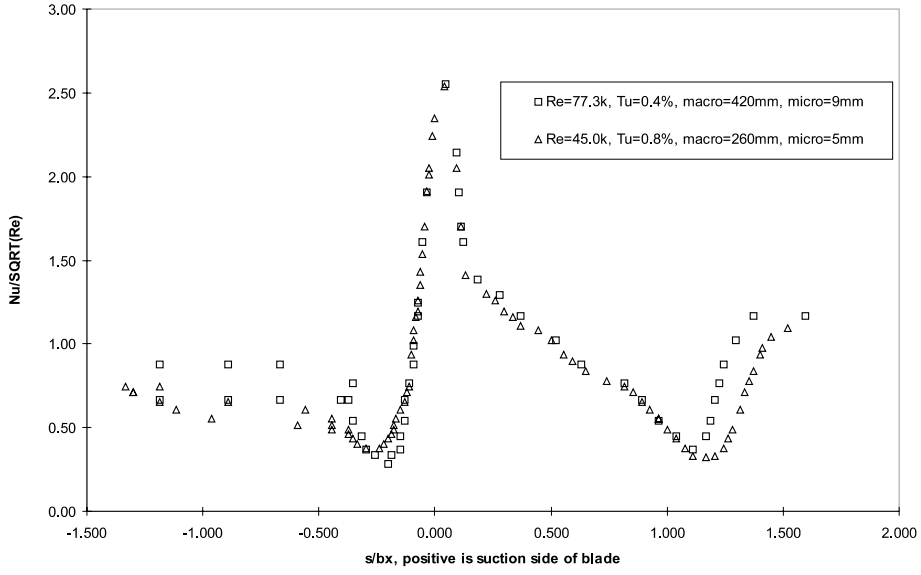

Fig. 9. Turbine blade heat transfer distributions for 77,300 and 45,000 Reynolds numbers.

6.2. Effect Reynolds number on turbine blade heat transfer

Fig. 9 shows that when the heat transfer distribution is plotted in terms of $Nu/Re^{0.5}$ the data will collapse in the laminar regions. For this clean tunnel data, it is clear that the only effect of increasing the Reynolds number is to move the separation point forward from $s/bx = 1.17$ to $s/bx = 1.11$ and Fig. 8 shows that the separation

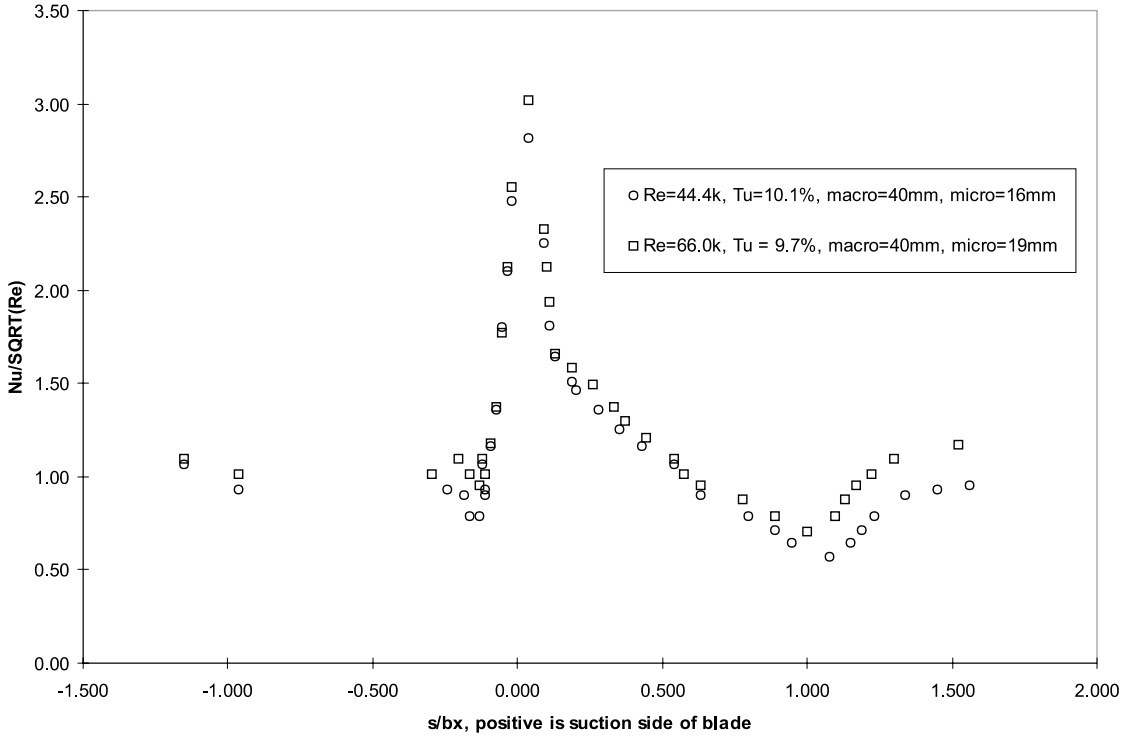

Fig. 10. Effect of Reynolds number on turbine blade heat transfer with 10% turbulence intensity using a 1.27-cm grid.

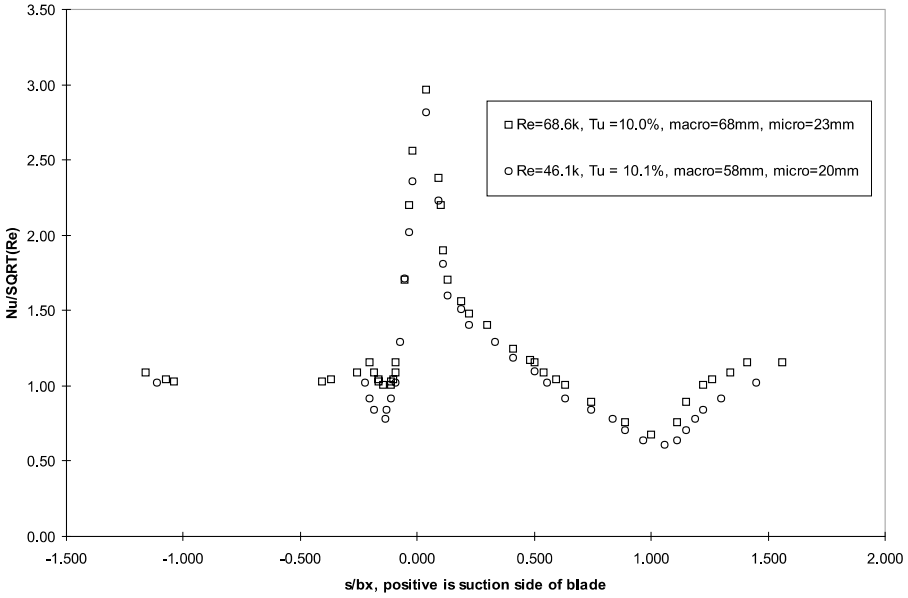

Fig. 11. Effect of Reynolds number on turbine blade heat transfer with 10% turbulence intensity using a 2.54-cm grid.

zone is much smaller at the higher Reynolds number condition.

Figs. 10–12 all show that increasing the Reynolds number will result in earlier transition and an amplification of the effect of elevated turbulence intensities. This is well known and has been reported by many researchers. It is easiest to measure this amplification at the stagnation point and this was shown in Fig. 4. Figs. 10–12 also reveal that the amplification is reduced for the present data as the turbulence length scales grow larger. This result is also discussed for the stagnation point heat transfer in Fig. 4.

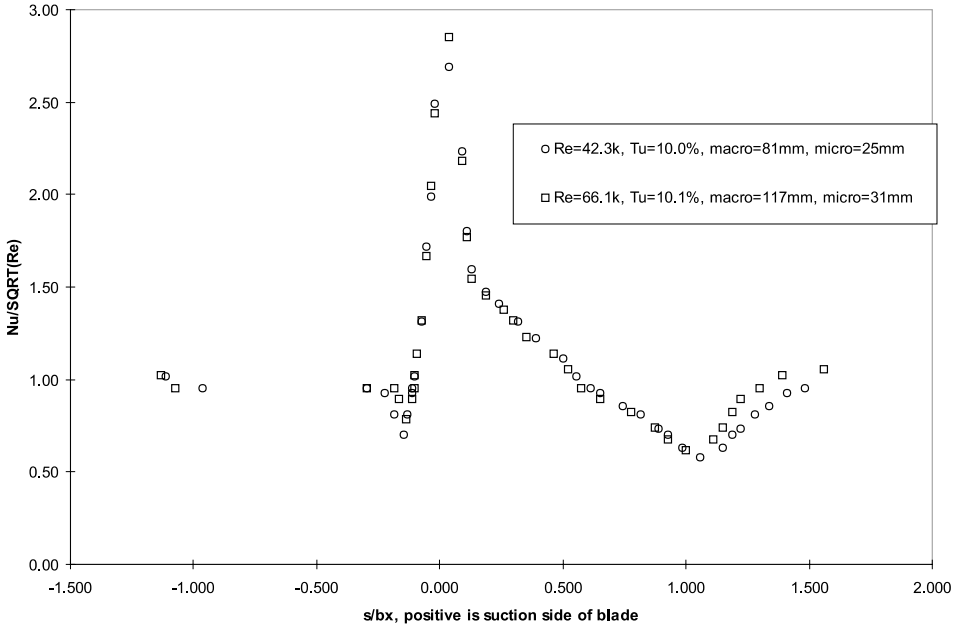

Fig. 12. Effect of Reynolds number on turbine blade heat transfer with 10% turbulence intensity using a 6.03-cm grid.

7. Conclusion

The effects of turbulence intensity, length scale, and Reynolds number on turbine blade heat transfer were investigated. Conclusions for turbulence intensity effects are:

- Increasing turbulence intensity from clean tunnel levels (0.4–0.8%) to 10% increased the stagnation heating at least 5.9% and up to 18.4%.
- For these low Reynolds number cases, on the suction surface the boundary layer always separated at low turbulence intensity (0.4–0.8%). Grid-generated turbulence (10%) prevented the separation and the boundary layer transitioned to turbulent. The laser tuft proved valuable in differentiating between boundary layer transition and separation within the low heat transfer bucket on the suction surface.
- On the pressure surface at low-turbulence intensity (0.4–0.8%), streaks of varying spanwise heat transfer were recorded. Either Görtler vortices or a three-dimensional transition process could potentially cause these streaks. The streaks were not present for the 10% turbulence cases and the pressure surface had a uniform transition location.

Conclusions for turbulence length scale effects are:

- For the grid generated turbulence (10%), stagnation heat transfer increased with smaller turbulence length scales, but an optimal length scale was not found.
- For this turbine blade shape the transition location did not depend on turbulence length scale. The transition location seems to be more dependent on pressure distribution, Reynolds number and turbulence intensity.
- The turbulence length scale did not have a measurable effect on the laminar boundary layer heat transfer on the suction surface.

Conclusions for Reynolds number effects are:

- For the 10% turbulence cases, increasing Reynolds number moved the transition location froward.
- For the clean tunnel cases (0.4–0.8%), increasing Reynolds number from 45,000 to 77,300 moved the boundary layer separation location slightly forward and decreased its length by 56%.
- The effect of increasing stagnation heat transfer due to turbulence intensity was amplified at higher Reynolds number.

Other findings were:

- Separation and transition locations corresponded to local minimums in heat transfer. Reattachment points did not correspond to local maximums in heat transfer, but instead, the heat transfer coefficient continued to rise downstream of the reattachment point.

The results presented in this paper show that turbulence length scale, in addition to intensity and Reynolds number have an important contribution to turbine blade aerodynamics and are important to CFD modelers who seek to predict boundary layer behavior in support of turbine blade design optimization efforts.

References

Baughn, J.W., Takahashi, R.K., Hoffman, M.A., McKillop, A.A., 1985. Local heat transfer measurements using an electrically heated thin gold-coated plastic sheet. ASME J. Heat Transfer 107, 953–959.

Baughn, J.W., Ireland, P.T., Jones, T.V., Saniei, N., 1989. A comparison of the transient and heated-coating methods for the measurements of the local heat transfer coefficients on a pin fin. ASME J. Heat Transfer 111, 877–881.

Baughn, J.W., Butler, R.J., Byerley, A.R., Rivir, R.B. 1995. An experimental investigation of heat transfer, transition and separation on turbine blades at low reynolds number and high turbulence intensity. ASME paper 95-WA/HT-25.

Blair, M.F., Dring, R.P., Joslyn, H.D., 1989a. The effects of turbulence and stator/rotor interactions on turbine heat transfer: Part 1. Design operating conditions. ASME J. Turbomach. 111, 87–96.

Blair, M.F., Dring, R.P., Joslyn, H.D., 1989b. The effects of turbulence and stator/rotor interactions on turbine heat transfer: Part 2. Effects of Reynolds number and incidence. ASME J. Turbomach. 111, 97–103.

Blair, M.F., 1994. An experimental study of heat transfer in a large-scale turbine rotor passage. ASME J. Turbomach. 116, 1–13.

Boyle, R.J., Russell, L.M., 1990. Experimental determination of stator endwall heat transfer. J. Turbomach. 112, 547–557.

Boyle, R.J., 1991. Navier–Stokes analysis of turbine blade heat transfer. J. Turbomach. 113, 392–403.

Cooper, T.E., Field, R.J., Meyer, J.F., 1975. Liquid crystal thermography and its application to the study of convective heat transfer. J. Heat Transfer, 442–450.

Crane, R.I., Sabzvari, J., 1989. Heat transfer visualization and measurement in unstable concave-wall laminar boundary layers. ASME J. Turbomach. 111, 51–56.

Dring, R.P., Blair, M.F., Joslyn, H.D., 1986. The effects of inlet turbulence and rotor stator interactions on the aerodynamic and heat transfer of a large-scale rotating turbine model, vol II. Heat transfer data tabulation. 15% Axial Spacing. NASA CR 179467, UTRC-R86-956480-2.

Dullenkopf, K., Mayle, R.E., 1994. The effects of incident turbulence and moving wakes on the laminar heat transfer in gas turbines. ASME J. Turbomach. 116, 23–28.

Dullenkopf, K., Schulz, A., Wittig, S., 1991. The effect of incident wake conditions on the mean heat transfer of an airfoil. J. Turbomach. 113, 412–418.

Giedt, W.H., 1949. Investigation of variation of point unit heat transfer coefficient around a cylinder normal to an air stream. Trans. ASME 71, 375–381.

Graziani, R.A., Blair, M.F., Taylor, J.R., Mayle, R.E., 1980. An experimental study of endwall and airfoil surface heat transfer in a large scale turbine blade cascade. J. Eng. Power 102, 257–267.

Hippensteele, S.A., Russell, L.M., Torres, F.J., 1985. Local heat-transfer measurements on a large scale-model turbine blade airfoil using a composite of a heater element and liquid crystals. J. Eng. Gas Power 107, 953–960.

Huang, P.G., Xiong, G. 1998. Transition and Turbulence Modeling of Low Pressure Turbine Flows. 36th Aerospace Sciences Meeting, Reno, AIAA 98-0339.

Kline, S.J., McKlintock, F.A., 1953. Describing uncertainties in single sample experiments. Mech. Eng. 75, 3–8.

Langston, L.S., Nice, M.L., Hooper, R.M., 1977. Three-dimensional flow within a turbine cascade passage. J. Eng. Power 99, 21–28.

Mayle, R.E., Dullenkopf, K., Schulz, A., 1997. The Turbulence that Matters. 1997 International Gas Turbine Conference, Orlando, ASME 97-GT-274.

Moore, J., Ransmayr, A., 1984a. Flow in a turbine cascade: Part 1. Losses and leading-edge effects. J. Eng. Gas Turbines Power 106, 401–408.

Moore, J., Ransmayr, A., 1984b. Flow in a turbine cascade: Part 2. Measurement of flow trajectories by ethylene detection. J. Eng. Gas Turbines Power 106, 409–413.

Moore, J., Adhye, R.Y., 1985. Secondary flows and losses downstream of a turbine cascade. J. Eng. Gas Turbines Power 107, 961–968.

Moore, J., Moore, J.G., 1985. Performance evaluation of linear turbine cascades using three-dimensional viscous flow calculations. J. Eng. Gas Turbines Power 107, 969–975.

Moore, J., Shaffer, D.M., Moore, J.G., 1987. Reynolds stresses and dissipation mechanisms downstream of a turbine cascade. J. Turbomach. 109, 258–267.

Murawski, C.G., Sondergaard, R., Rivir, R.B., Simon, T.W., Vafai, K., Volino, R.J. 1997. Experimental Study of the Unsteady Aerodynamics in a Linear Cascade with Low Reynolds Number Low Pressure Turbine Blades. 1997 International Gas Turbine Conference, Orlando, ASME 97-GT-95.

O'Brien, J.E., Simoneau, R.J., LaGraff, J.E., Morehouse, K.A. 1986. Unsteady Heat Transfer and Direct Comparison for Steady-State Measurements in a Rotor-Wake Experiment. Proceedings of the Eighth International Heat Transfer Conference, San Francisco, pp. 1243–1248.

Rivir, R.B., Johnston, J.P., Eaton, J.K., 1994. Heat transfer on a flat surface under a region of turbulent separation. J. Turbomach. 116, 57–62.

Rivir, R.B. 1996. Transition on turbine blades and cascades at low Reynolds numbers. AIAA 96-2079.

Roach, P.E., 1987. The generation of nearly isotropic turbulence by means of grids. Heat Fluid Flow 8 (2), 82–92.

Simonich, J.C., Bradshaw, P., 1978. Effect of free-stream turbulence on heat transfer through a turbulent boundary layer. ASME J. Heat Transfer 100, 671–677.

Van Fossen, G.J., Simoneau, R.J., Ching, C.Y., 1995. Influence of turbulence parameters, Reynolds number, and body shape on stagnation-region heat transfer. ASME J. Heat Transfer 117, 597–603.

Wilson, D.G., Pope, J.A., 1954. Convective heat transfer to gas turbine blade surfaces. Proc. Inst. Mech. Eng. 168, 861–874.

Zhang, L., Han, J.C., 1994. Influence of mainstream turbulence on heat transfer coefficients from a gas turbine blade. J. Heat Transfer 116, 896–903.